JCI insight

# Registration of the extracellular matrix components constituting the fibroblastic focus in idiopathic pulmonary fibrosis

Jeremy Herrera, … , Craig A. Henke, Peter B. Bitterman

*JCI Insight.* 2019;4(1):e125185. https://doi.org/10.1172/jci.insight.125185.

**Research Article** **Pulmonology**

The extracellular matrix (ECM) in idiopathic pulmonary fibrosis (IPF) drives fibrosis progression; however, the ECM composition of the fibroblastic focus (the hallmark lesion in IPF) and adjacent regions remains incompletely defined. Herein, we serially sectioned IPF lung specimens constructed into tissue microarrays and immunostained for ECM components reported to be deregulated in IPF. Immunostained sections were imaged, anatomically aligned, and 3D reconstructed. The myofibroblast core of the fibroblastic focus (defined by collagen I, α-smooth muscle actin, and procollagen I immunoreactivity) was associated with collagens III, IV, V, and VI; fibronectin; hyaluronan; and versican immunoreactivity. Hyaluronan immunoreactivity was also present at the fibroblastic focus perimeter and at sites where early lesions appear to be forming. Fibrinogen immunoreactivity was often observed at regions of damaged epithelium lining the airspace and the perimeter of the myofibroblast core but was absent from the myofibroblast core itself. The ECM components of the fibroblastic focus were distributed in a characteristic and reproducible manner in multiple patients. This information can inform the development of high-fidelity model systems to dissect mechanisms by which the IPF ECM drives fibrosis progression.



JCI insight

RESEARCH ARTICLE

# Registration of the extracellular matrix components constituting the fibroblastic focus in idiopathic pulmonary fibrosis

**Jeremy Herrera,[1] Colleen Forster,[2] Thomas Pengo,[3] Angeles Montero,[4] Joe Swift,[1] Martin A. Schwartz,[1] Craig A. Henke,[5] and Peter B. Bitterman[5]**

[1]Wellcome Centre for Cell-Matrix Research, Manchester Academic Health Science Centre, University of Manchester, Manchester, United Kingdom. [2]University of Minnesota, Clinical and Translational Science Institute, Minneapolis, Minnesota, USA. [3]University of Minnesota Informatics Institute, University of Minnesota Twin Cities, Minneapolis, Minnesota, USA. [4]Manchester University Foundation Trust, Department of Histopathology, Manchester, United Kingdom. [5]University of Minnesota, Department of Medicine, Minneapolis, Minnesota, USA.

**The extracellular matrix (ECM) in idiopathic pulmonary fibrosis (IPF) drives fibrosis progression; however, the ECM composition of the fibroblastic focus (the hallmark lesion in IPF) and adjacent regions remains incompletely defined. Herein, we serially sectioned IPF lung specimens constructed into tissue microarrays and immunostained for ECM components reported to be deregulated in IPF. Immunostained sections were imaged, anatomically aligned, and 3D reconstructed. The myofibroblast core of the fibroblastic focus (defined by collagen I, α-smooth muscle actin, and procollagen I immunoreactivity) was associated with collagens III, IV, V, and VI; fibronectin; hyaluronan; and versican immunoreactivity. Hyaluronan immunoreactivity was also present at the fibroblastic focus perimeter and at sites where early lesions appear to be forming. Fibrinogen immunoreactivity was often observed at regions of damaged epithelium lining the airspace and the perimeter of the myofibroblast core but was absent from the myofibroblast core itself. The ECM components of the fibroblastic focus were distributed in a characteristic and reproducible manner in multiple patients. This information can inform the development of high-fidelity model systems to dissect mechanisms by which the IPF ECM drives fibrosis progression.**

## Introduction

Idiopathic pulmonary fibrosis (IPF) is a lethal disease characterized by deposition of a pathological extracellular matrix (ECM) that establishes a positive feedback loop that mediates fibrosis progression (1). Lung ECM from IPF patients (IPF ECM) is sufficient to drive myofibroblast differentiation of fibroblasts derived from nonfibrotic lungs (2, 3). IPF ECM increases ribosome recruitment to hundreds of stromal transcripts, indicative of increased translation (4). Some of these effects can be explained by the ability of IPF ECM to decrease Dicer1, a core component of the microRNA-processing machinery (5), which suppresses biogenesis of microRNA-29, a master negative regulator of stromal genes. Left unknown is the identity of those components of the IPF ECM that promote fibrosis progression.

Whole lung proteomic studies identified differences between IPF ECM and control lung ECM (2, 6–8). However, IPF is a spatially heterogeneous disease and ECM components show regional variations (9). To understand how the ECM might drive fibrosis progression, an important step will be to characterize the ECM in the specific regions where collagen is being actively synthesized. A landmark study by Kuhn and McDonald identified the fibroblastic focus, the hallmark lesion in IPF, as the locus of active ECM deposition (10). Subsequent reports identified the location of several ECM constituents in the IPF lung. However, there are no studies that have systematically registered each of these ECM components to one another in and around the fibroblastic focus.

Fibroblastic foci are polarized structures containing a myofibroblast core, which is the major site of collagen synthesis, and an active fibrotic front where proliferating progenitor cells reside at sites of thickened alveolar septa encroaching into morphologically normal lung (11). Characterizing the composition of these two regions is an important step toward understanding the mechanism by which

**Conflict of interest:** The authors have declared that no conflict of interest exists.



**Submitted:** October 1, 2018
**Accepted:** November 20, 2018
**Published:** January 10, 2019

**Reference information:**
*JCI Insight*. 2019;4(1):e125185.
https://doi.org/10.1172/jci.insight.125185.

IPF ECM drives fibrosis progression. We therefore combined immunohistochemical analysis of tissue arrays with 3D reconstruction to define the anatomic relationships among the ECM constituents of the fibroblastic focus and adjacent regions of the IPF lung. Our data indicate that all fibroblastic foci share the same ECM components in the same distribution, consistent with a conserved role for the ECM in the pathogenesis of fibrosis progression. This study will help inform future research to understand ECM-mediated mechanisms of fibrosis progression.

## Results

*The myofibroblast core of the fibroblastic focus contains cells expressing αSMA and procollagen I in a collagen I–rich ECM*. We have previously reported that the core of the fibroblastic focus is defined by the expression of procollagen I, a marker for active collagen I synthesis (5, 11). It has also been reported that α-smooth muscle actin–positive (αSMA-positive) cells (12, 13) and collagen I (12, 14) are present within the fibroblastic focus. We serially sectioned IPF lung specimens and confirmed the presence of collagen I, αSMA, and procollagen I immunoreactivity in what we define as the myofibroblast core of the fibroblastic focus (Figure 1). Low-magnification images of 2 IPF specimens illustrate that regions of collagen I expression overlap with αSMA and procollagen I immunoreactivity (Figure 1A); higher-magnification images of 3 IPF specimens show that both αSMA and procollagen I are present in the collagen I–rich myofibroblast core (Figure 1B, red dotted lines outline the myofibroblast core). Quantification shows that, in all cases, collagen I immunoreactivity associated with both αSMA and procollagen I (Figure 1C, $n$ = 12 IPF specimens, $n$ = 29 fibroblastic foci per immunostain).

We found collagen I immunoreactivity within the myofibroblast core (region of procollagen I positivity) and particularly within regions of thickened alveolar septa (the active fibrotic front) at the interface of the myofibroblast core and morphologically normal alveolar structures (11). However, collagen I immunoreactivity was less prominent within morphologically normal alveolar structures. In contrast, αSMA immunoreactivity is not restricted to the myofibroblast core. We observed αSMA expression within thickened alveolar septa and within adjacent morphologically normal alveolar structures. Procollagen I expression sharply demarcated the myofibroblast core of the fibroblastic focus. Taken together, these findings support a definition of the myofibroblast core of the fibroblastic focus as a region with myofibroblasts expressing αSMA and procollagen I, consistent with active collagen synthesis, embedded in a collagen I–rich ECM.

In order to reconstruct a 3D image of the fibroblastic focus, IPF specimens were serially sectioned at 5 μm and immunostained for collagen I, αSMA, and procollagen I for up to 3 immunostains each (9 serial sections spanning 45 μm). Each immunostain was unmixed and pseudocolored. A 3D reconstruction was performed by arranging each serial component at its estimated position in a vertical stack (Supplemental Figure 1 and Supplemental Video 1; supplemental material available online with this article; https://doi.org/10.1172/jci.insight.125185DS1).

*Collagen V and hyaluronan*. Collagen V expression is increased in the IPF lung (15), and birefringence analysis suggests that collagen V is expressed within the fibroblastic focus (16). Hyaluronan has also been observed within the fibroblastic focus (17, 18). We found signal for both collagen V and hyaluronan in the collagen I–rich myofibroblast core of the fibroblastic focus (Figure 2; $n$ = 8 IPF specimens, 40 fibroblastic foci per immunostain). A 3D reconstruction is shown in Supplemental Figure 2 and Supplemental Video 2.

We next examined regions immediately adjacent to the myofibroblast core and found collagen V and hyaluronan within thickened alveolar septa. In addition, whereas collagen V was expressed within morphologically normal alveolar structures adjacent to the fibroblastic focus, hyaluronan was not. These data indicate that hyaluronan is predominantly localized to the periphery of the fibroblastic focus and is found in areas where early lesions appear to be forming (Figure 3).

*Fibronectin and collagen VI*. Both fibronectin and collagen VI are reported to be expressed within the fibroblastic focus (10, 19–21). We found signal for both fibronectin and collagen VI in the collagen I–rich myofibroblast core of the fibroblastic focus (Figure 4, $n$ = 8 IPF specimens, 41 fibroblastic foci per immunostain). In addition, both fibronectin and collagen VI were found within thickened alveolar septa and within adjacent morphologically normal alveolar structures. A 3D reconstruction is shown in Supplemental Figure 3 and Supplemental Video 3.

*Collagen IV and versican*. The current literature regarding collagen IV within the fibroblastic focus remains inconclusive. Some reports show that when costained with procollagen I, collagen IV does

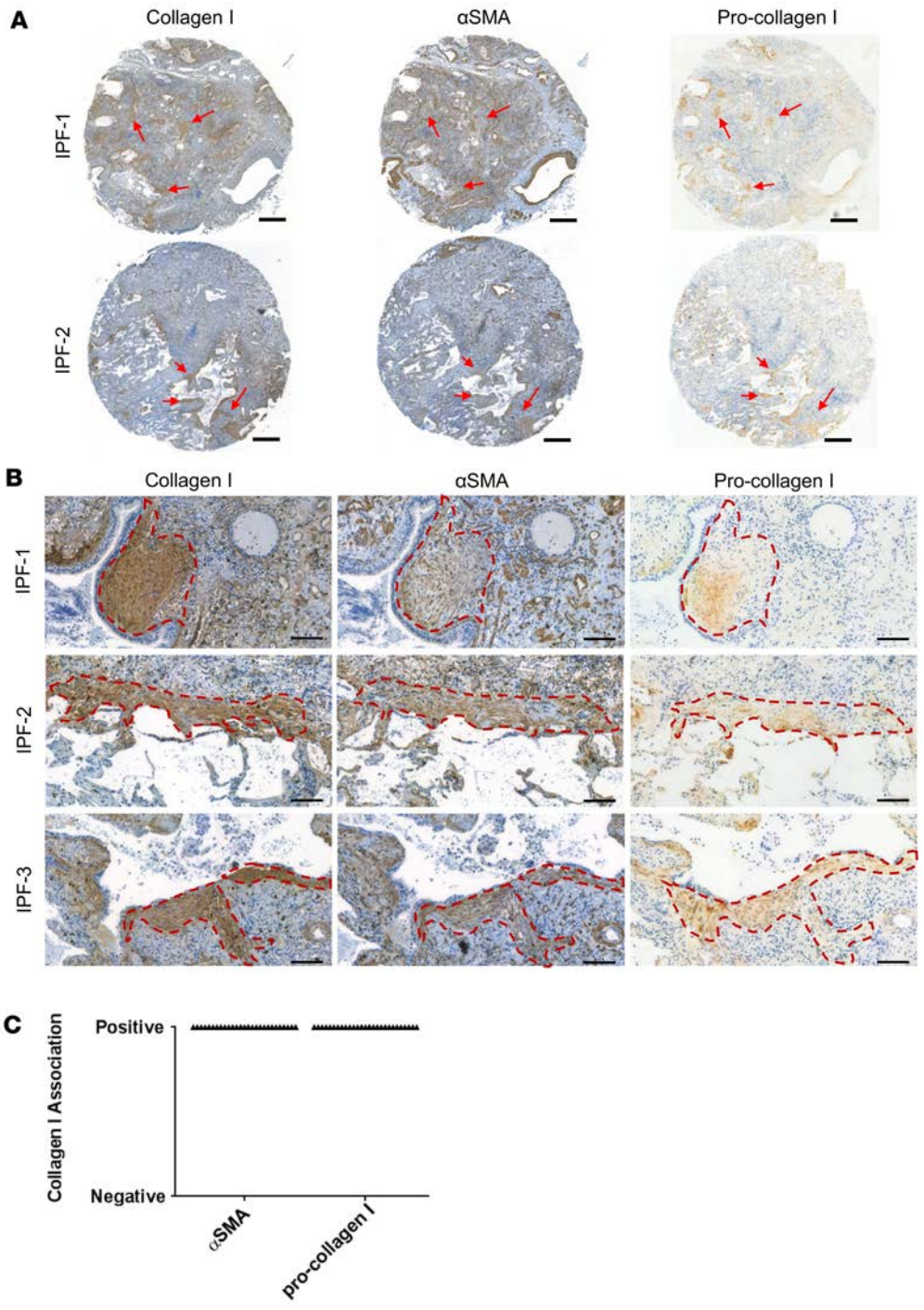


**Figure 1. The myofibroblast core of the fibroblastic focus is defined by collagen I and cells expressing α-smooth muscle actin and procollagen I.** (**A** and **B**) Twelve IPF specimens were assembled into a tissue microarray, serially sectioned at 5 μm, and immunostained for collagen I (left), α-smooth muscle actin (αSMA; middle), and procollagen I (right). (**A**) Low-magnification images of 2 IPF specimen serial section core punches. Red arrows show regions of high collagen I deposition traced through the serial stains. Scale bar: 500 μm. (**B**) High-magnification images of 3 IPF specimens. The myofibroblast core of the fibroblastic focus is outlined by red dotted lines. Scale bar: 100 μm. (**C**) The myofibroblast core of the fibroblastic focus, characterized by collagen I immunoreactivity, was scored as either positive (score = 1) or negative (score = 0) immunoreactivity for αSMA or procollagen I. Each myofibroblast core was serially immunostained up to 4 times for αSMA and procollagen I, and their averaged score is represented as a single data point on the graph. A $\chi^2$ test was performed for αSMA and procollagen I association with collagen I; $P = 0.9999$ for both ($n = 29$ fibroblastic foci for αSMA, $n = 29$ fibroblastic foci for procollagen I; $n = 12$ IPF patients total [1–6 fibroblastic foci per patient]).

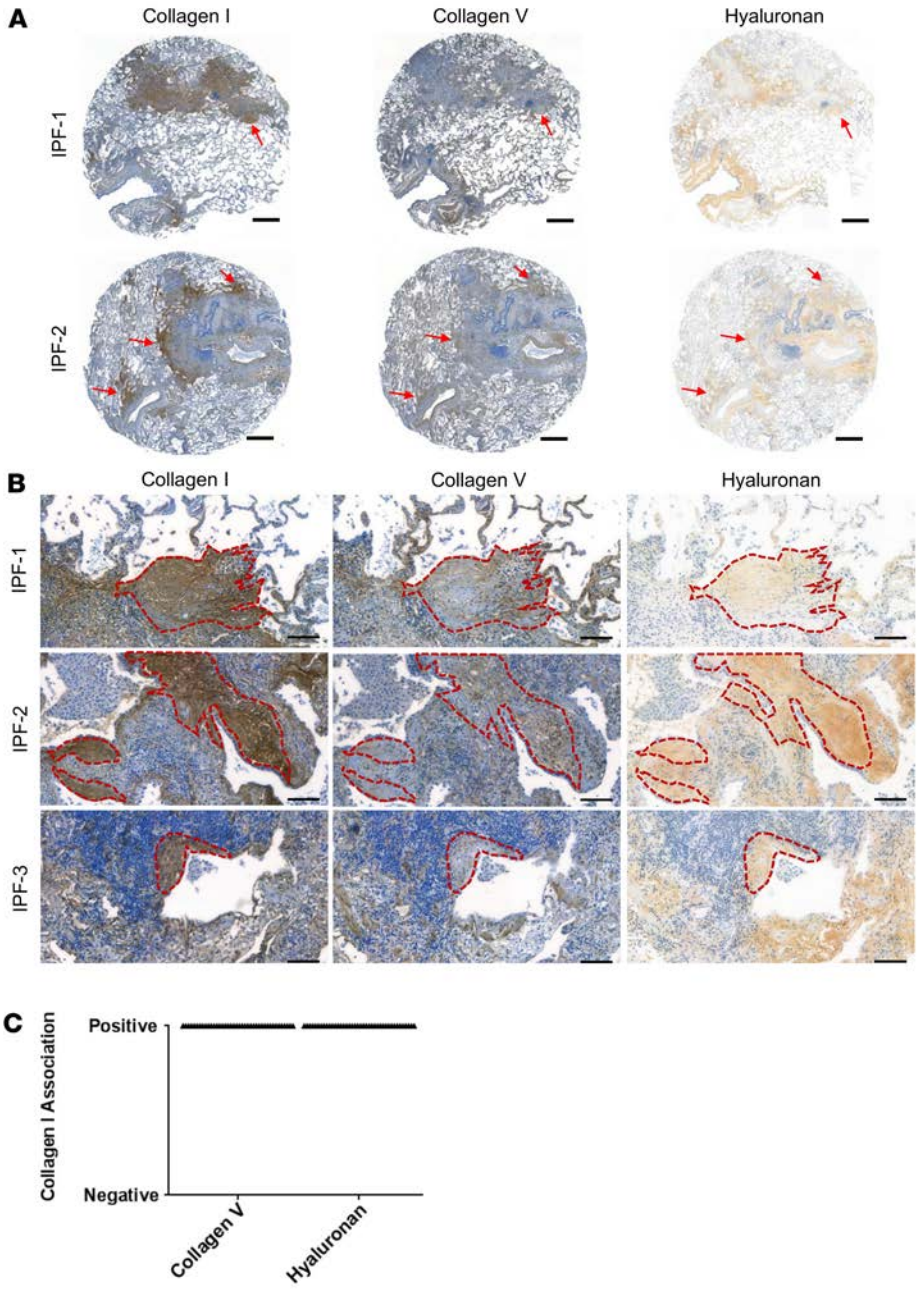


**Figure 2. Distribution of collagen V and hyaluronan in the fibroblastic focus.** (**A** and **B**) Twelve IPF specimens were assembled into a tissue microarray, serially sectioned at 5 μm, and immunostained for collagen I (left), collagen V (middle), and hyaluronan (right). (**A**) Low-magnification images of 2 IPF specimen serial section core punches. Red arrows show regions of high collagen I deposition traced through the serial stains. Scale bar: 500 μm. (**B**) High-magnification images of 3 IPF specimens. Each myofibroblast core of the fibroblastic focus is outlined by a red dotted line. Scale bar: 100 μm. (**C**) The myofibroblast core of the fibroblastic focus, characterized by collagen I immunoreactivity, was scored as either positive (score = 1) or negative (score = 0) immunoreactivity for collagen V or hyaluronan. Each myofibroblast core was serially immunostained up to 4 times for collagen V and hyaluronan, and their averaged score is represented as a single data point on the graph. A $\chi^2$ test was performed for collagen V and hyaluronan association with collagen I; $P = 0.9999$ for both ($n = 40$ fibroblastic foci for collagen V, $n = 40$ fibroblastic foci for hyaluronan; $n = 9$ IPF patients total [1–7 fibroblastic foci per patient]).

not colocalize; instead, collagen IV localizes to the outer perimeter of the fibroblastic focus lining the alveolar epithelium (19). Another report showed staining within the fibroblastic focus (22), and another report described collagen IV staining as uneven, multilayered, and focally disrupted within the fibroblastic focus (23). In contrast, versican is found within the fibroblastic focus (17).

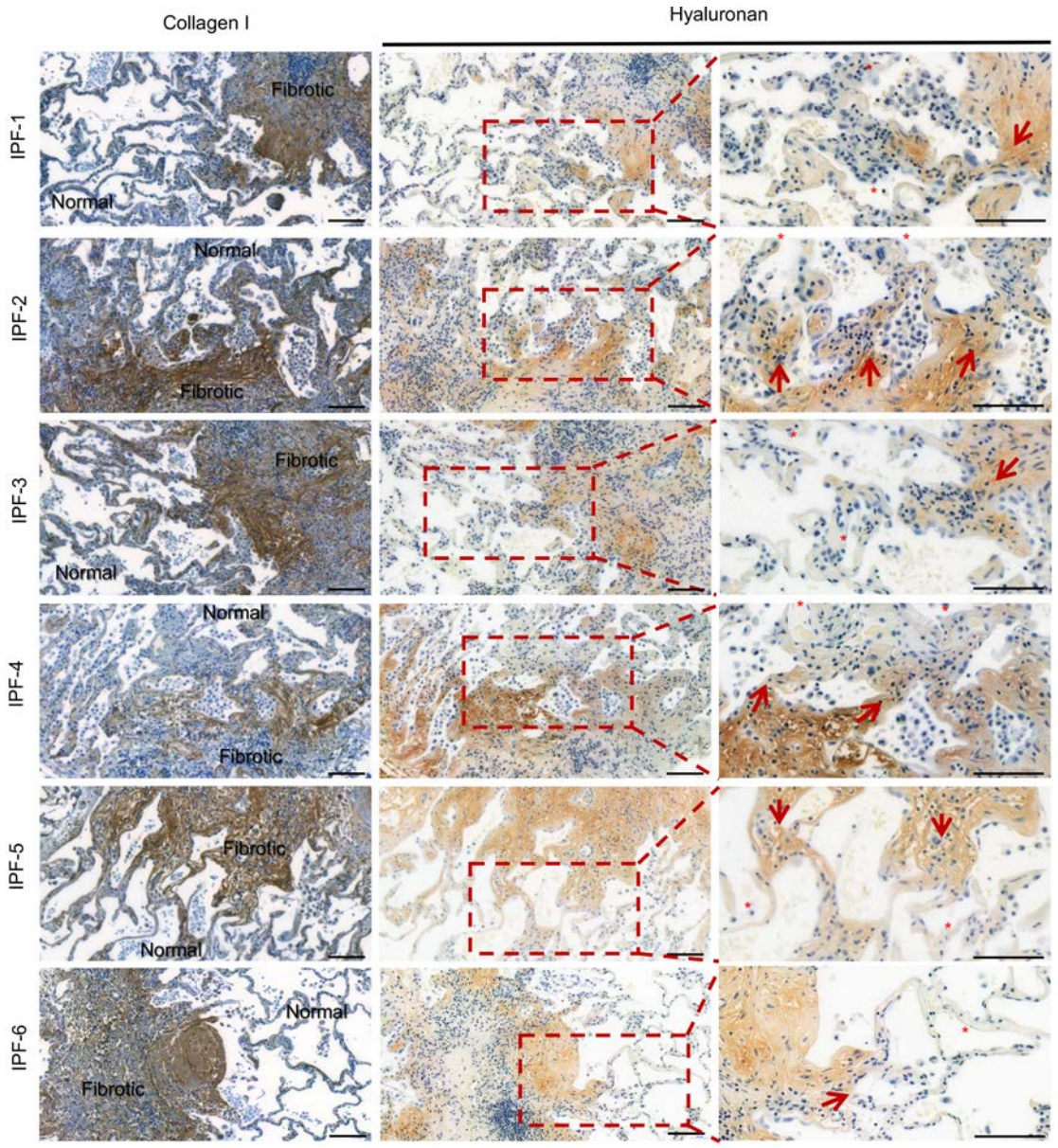


**Figure 3. Hyaluronan is present at the interface between fibrotic and morphologically normal alveoli and absent from morphologically normal alveolar walls.** FFPE serial sections of 6 IPF specimens were stained for collagen I (left) and hyaluronan (middle), with a higher-magnification inset for hyaluronan (right). Shown are specimens with a fibrotic and normal interphase highlighted on the collagen I immunostain (left). High magnification of the hyaluronan stain shows strong reactivity (right, red arrows) along the active fibrotic front (thickened alveolar septa), with gradual attenuation of reactivity as it transitions into normal alveoli (red asterisk). Scale bar: 100 μm.

We found that both collagen IV and versican were present within the collagen I–rich myofibroblast core (Figure 5, $n = 9$ IPF specimens, 53 fibroblastic foci per immunostain). Collagen IV immunoreactivity in 23 of 53 (43%) of the myofibroblast cores examined appeared patchy or layered along the epithelium in accord with previous reports showing an uneven, multilayered, and focally disrupted staining pattern (23). In 30 of 53 (57%) myofibroblast cores examined, we observed signal throughout the myofibroblast core in accord with other reports (22) (more examples in Supplemental Figure 4). Collagen IV and versican were present in thickened alveolar septa and adjacent morphologically normal alveolar structures. A 3D reconstruction is shown in Supplemental Figure 5 and Supplemental Video 4.

*Collagen III and fibrinogen*. Collagen III has been reported to be within the fibroblastic focus (14); however, localization of fibrinogen, a marker of active tissue injury, is less well defined. Fibrin, the mature form of fibrinogen, is associated with type II epithelial cells in the IPF lung (24); but its relationship to

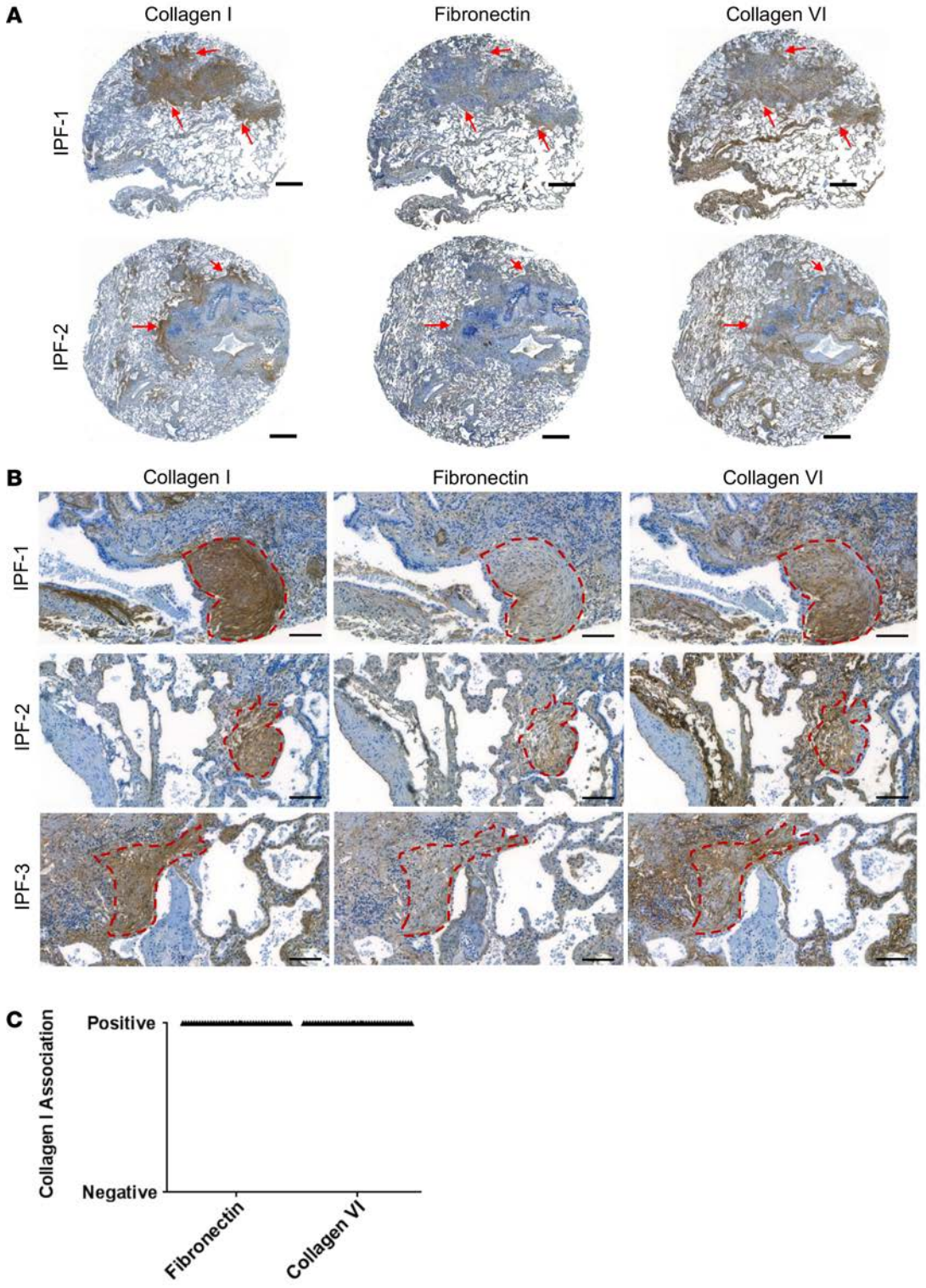


**Figure 4. Distribution of fibronectin and collagen VI in the fibroblastic focus.** (**A** and **B**) Twelve IPF specimens were assembled into a tissue microarray, serially sectioned at 5 μm, and immunostained for collagen I (left), fibronectin (middle), and collagen VI (right). (**A**) Low-magnification images of 2 IPF specimen serial section core punches. Red arrows show regions of high collagen I deposition traced through the serial stains. Scale bar: 500 μm. (**B**) High-magnification images of 3 IPF specimens. The myofibroblast core of the fibroblastic focus is outlined by a red dotted line. Scale bar: 100 μm. (**C**) The myofibroblast core of the fibroblastic focus, characterized by collagen I immunoreactivity, was scored as either positive (score = 1) or negative (score = 0) immunoreactivity for fibronectin or collagen VI. Each myofibroblast core was serially immunostained up to 4 times for fibronectin and collagen VI, and their averaged score is represented as a single data point on the graph. A $\chi^2$ test was performed for fibronectin and collagen VI association with collagen I; $P = 0.9999$ for both ($n = 41$ fibroblastic foci for fibronectin, $n = 41$ fibroblastic foci for collagen VI; $n = 9$ IPF patients total [2–8 fibroblastic foci per patient]).

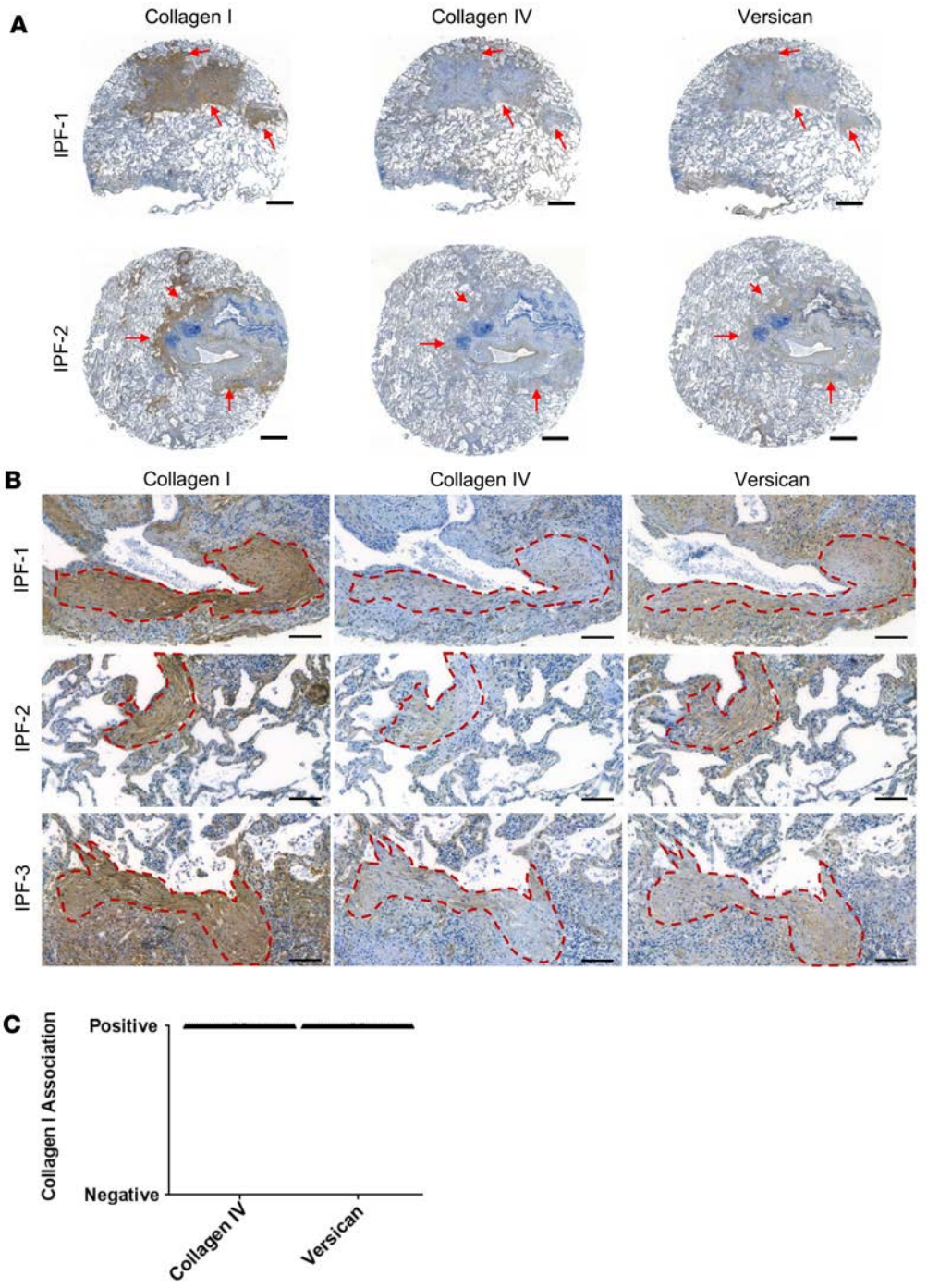


**Figure 5. Distribution of collagen IV and versican in the fibroblastic focus.** (**A** and **B**) Twelve IPF specimens were assembled into a tissue microarray, serially sectioned at 5 μm, and immunostained for collagen I (left), collagen IV (middle), and versican (right). (**A**) Low-magnification images of 2 IPF specimen serial section core punches. Red arrows show regions of high collagen I deposition traced through the serial stains. Scale bar: 500 μm. (**B**) High-magnification images of 3 IPF specimens. The myofibroblast core of the fibroblastic focus is outlined by a red dotted line. Scale bar: 100 μm. (**C**) The myofibroblast core of the fibroblastic focus, characterized by collagen I immunoreactivity, was scored as either positive (score = 1) or negative (score = 0) immunoreactivity for collagen IV or versican. Each myofibroblast core was serially immunostained up to 4 times for collagen IV and versican, and their averaged score is represented as a single data point on the graph. A $\chi^2$ test was performed for collagen IV and versican association with collagen I; $P$ = 0.9999 for both ($n$ = 53 fibroblastic foci for collagen IV, $n$ = 53 fibroblastic foci for versican; $n$ = 9 IPF patients total [1–10 fibroblastic foci per patient]).

the fibroblastic focus has not been documented. A separate study reported inconsistent staining in the fibroblastic focus but high immunoreactivity in IPF airways (19). We observed collagen III in the collagen I–rich myofibroblast core, whereas fibrinogen was absent from this region (Figure 6, $n = 7$ IPF specimens, 24 fibroblastic foci per immunostain). Collagen III was present within thickened alveolar septa and within adjacent morphologically normal alveolar structures. Fibrinogen immunoreactivity was found throughout the IPF lung. Fibrinogen immunoreactivity was often observed at regions of damaged epithelium lining the airspace and at the perimeter of the myofibroblast core (Figure 7). Fibrinogen was absent from adjacent thickened alveolar septa and absent within the interstitium of morphologically normal alveolar structures. A 3D reconstruction is shown in Supplemental Figure 6 and Supplemental Video 5.

## Discussion

The fibroblastic focus is a polarized structure containing a myofibroblast core comprising nonproliferating myofibroblasts (25, 26) and an active cellular fibrotic front that includes activated macrophages (27) and proliferating mesenchymal progenitor cells (11). Our present knowledge supports the inference that the fibroblastic focus is a dynamic structure, where, in time, the mesenchymal progenitor cell population invades adjacent normal alveolar interstitium, differentiates into fibrogenic myofibroblasts, and gives rise to new fibroblastic foci, leaving behind a highly remodeled ECM. This process may be driven, in part, by a fibrogenic ECM (4).

Using immunostaining and 3D reconstruction of IPF lung specimens in tissue microarrays (TMAs), here we report the relationships among ECM components registered to the regions of the fibroblastic focus. We show that collagens I, III, IV, V, and VI; fibronectin; and versican are localized to the myofibroblast core of the fibroblastic focus, within adjacent thickened alveolar septa (active fibrotic front) and within normal alveolar septa. In contrast, hyaluronan is present in the myofibroblast core of the fibroblastic focus, at the perimeter of the fibroblastic focus, and in areas where early lesions appear to be forming. Fibrinogen was regularly observed along the damaged and disrupted epithelial lining of the myofibroblast core. We speculate that both hyaluronan and fibrinogen may be involved in the mechanisms driving fibrosis progression (Figure 8).

In this report, we show that hyaluronan localizes within the collagen I–rich myofibroblast core and to the periphery of the fibroblastic focus. This localization pattern is unique among the ECM components that we examined. Hyaluronan is a profibrotic ECM component found to promote mesenchymal progenitor cell migration (28) and enhance cell invasion (29). This supports the idea that hyaluronan may participate in lung mesenchymal progenitor cell invasion into adjacent normal alveolar structures. Hyaluronan also promotes collagen expression in vitro (30), causes de novo collagen synthesis in vivo after injection into human forearm skin (31, 32), globally regulates microRNA expression in vivo (33), and can specifically regulate microRNA-29, a major negative regulator of ECM genes, in Kupffer cells (34). These data support the speculation that hyaluronan may be part of the mechanism leading to the abnormal fibroblast Dicer1/miR-29/collagen I signaling axis in IPF (5).

In accord with a model of IPF as abnormal wound healing (35), we show that fibrinogen is present at regions of epithelial damage/stress, lining the myofibroblast core and airspace interface. It has been previously shown that tissue factor (a main initiator of the coagulation pathway) is expressed at the damaged/stressed epithelium overlying the myofibroblast core and airspace interface (24). Tissue factor expression stimulates conversion of soluble fibrinogen to insoluble fibrin, consistent with fibrinogen immunostaining in peripheral regions, but is absent in the myofibroblast core of the fibroblastic focus. Fibrinogen/fibrin exert much of their biological activity through binding to integrin αvβ3, which is known to stimulate cell proliferation and migration (36, 37). Thus, the fibrinogen coating along the myofibroblast core could contribute to ECM-mediated fibrosis invasion into airspaces.

In the current study, we localized multiple ECM components known to be deregulated in IPF. One limitation of the experimental design is that peroxidase-based immunostaining reactions are not quantitative; therefore, we cannot determine relative levels of each ECM component. This limitation could be addressed via proteomic analysis of laser-microdissected samples from IPF lung or by matrix-assisted laser desorption/ionization (38), which would complement the present study. Another limitation of our study is that staining cannot determine the molecular weight of hyaluronan within the fibroblastic focus. Hyaluronan can range in size from $2 \times 10^3$ up to $10^7$ daltons (39, 40). In some biological settings, the size of hyaluronan can determine its function; and covalent modifications of hyaluronan into heavy chains has been shown to mediate pathological processes (41). Finally, immunostaining does not provide information about the nanoscale topography, organization, orientation and polarization of the ECM, which may have strong effects on biological functions (42).

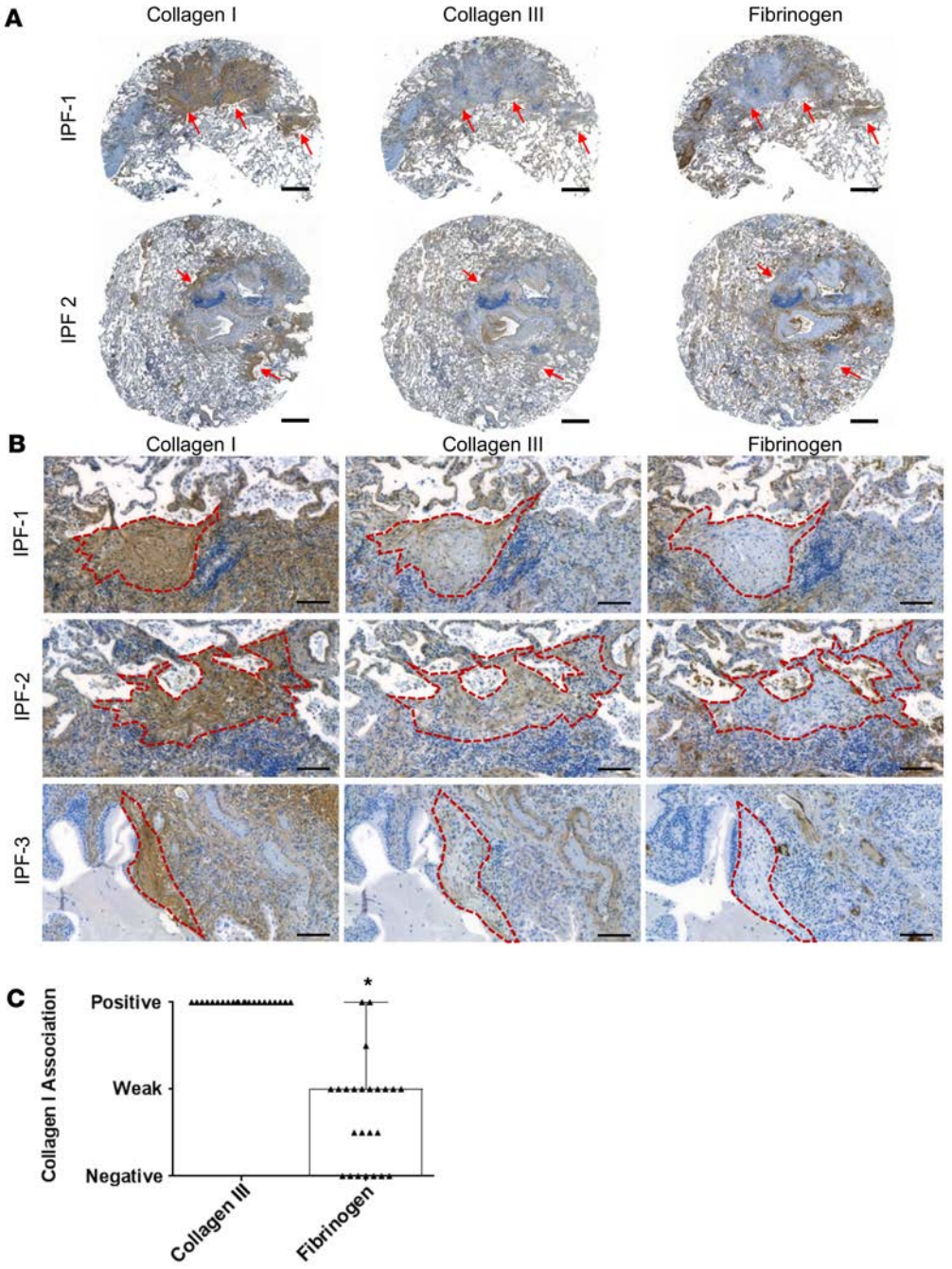


**Figure 6. Distribution of collagen III and fibrinogen in the fibroblastic focus.** (**A** and **B**) Twelve IPF specimens were assembled into a tissue microarray, serially sectioned at 5 μm, and immunostained for collagen I (left), collagen III (middle), and fibrinogen (right). (**A**) Low-magnification images of 2 IPF specimen serial section core punches. Red arrows show regions of high collagen I deposition traced through the serial stains. Scale bar: 500 μm. (**B**) High-magnification images of 3 IPF specimens. The myofibroblast core of the fibroblastic focus is outlined by a red dotted line. Scale bar: 100 μm. (**C**) The myofibroblast core of the fibroblastic focus, characterized by collagen I immunoreactivity, was scored as positive (score = 1), weak (score = 0.5), or negative (score = 0) immunoreactivity for collagen III or fibrinogen. Each myofibroblast core was serially immunostained up to 4 times for collagen III and fibrinogen, and their averaged score is represented as a single data point on the graph. A $\chi^2$ test was performed for collagen III and fibrinogen association with collagen I; *$P < 0.0001$ ($n$ = 22 fibroblastic foci for collagen III, $n$ = 24 fibroblastic foci for fibrinogen; $n$ = 7 IPF patients total [1–4 fibroblastic foci per patient]).

Our work represents an important step toward the creation of a comprehensive tissue atlas for IPF. Such an atlas will inform the development of ECM model systems with the correct mechanics, cell types, ECM types, organization, and orientation needed to elucidate the mechanisms by which the ECM drives fibrosis progression in IPF.

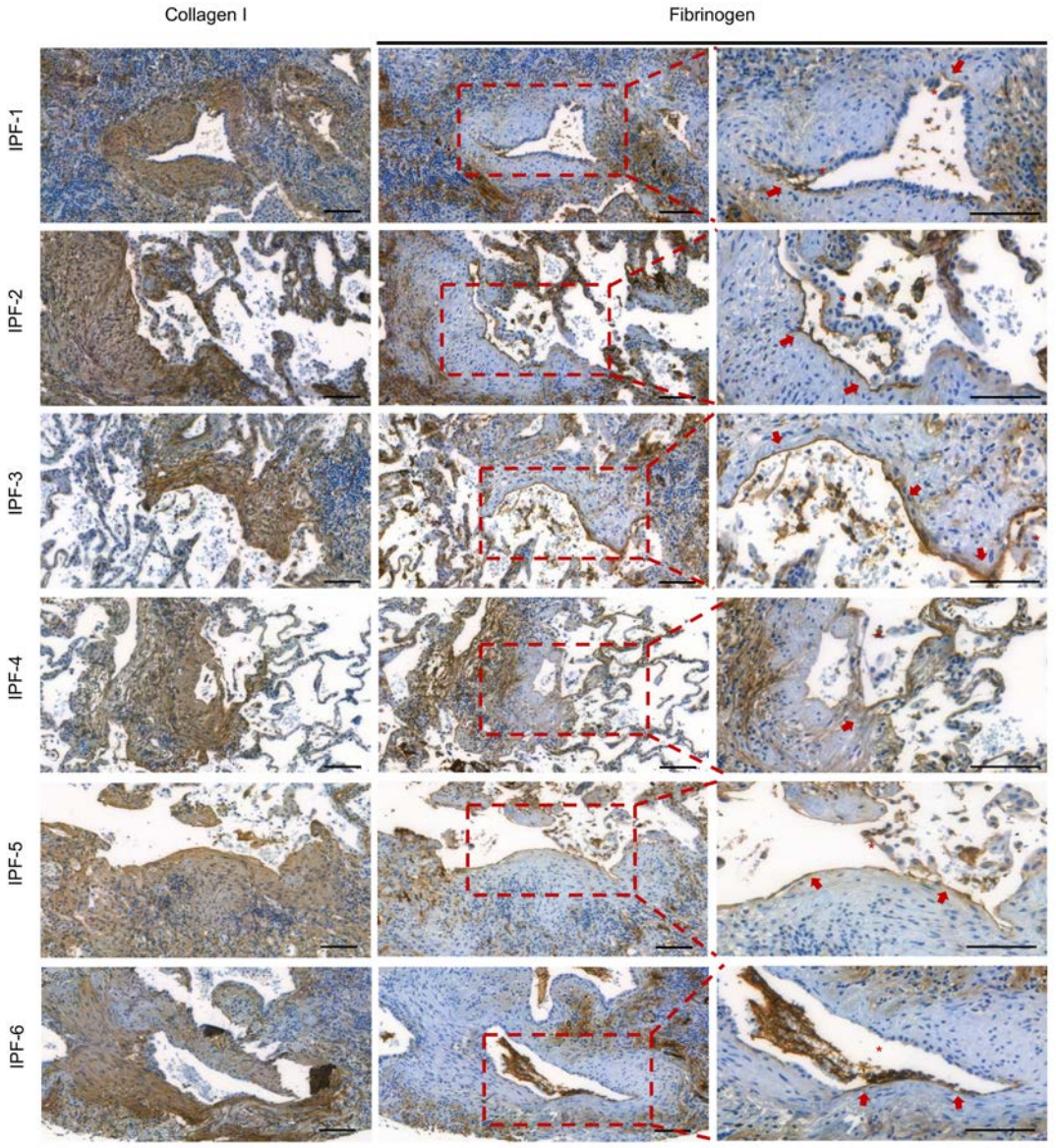


**Figure 7. Fibrinogen is expressed at the interface between the myofibroblast core and small airways**. FFPE sections of 6 IPF specimens were sectioned and immunostained for collagen I (left) and fibrinogen (middle), with a higher-magnification inset (right). Higher magnification reveals strong fibrinogen immunoreactivity (right, red arrows) along the interface between the myofibroblast core and airspace, where there is evidence of damage to the epithelium (red asterisk). Scale bar: 100 μm.

## Methods

*Human lung procurement*. Human lung tissue was procured after explant or during biopsy and deidentified by the University of Minnesota Biological Materials Procurement Network (BioNet). All specimens came from patients meeting established criteria for the diagnosis of IPF and carried a final pathological diagnosis of usual interstitial pneumonia (43, 44).

*Immunohistochemistry*. Human lung samples were formalin fixed and paraffin embedded (FFPE), followed by TMA construction using 4-mm core punches. Deparaffinized and rehydrated 5-μm serial sections were subjected to antigen heat retrieval using citrate buffer, pH 6.0 (BioCare, RV1000), for 30 minutes at 100°C, were allowed to cool to room temperature for 20 minutes, and were rinsed in running tap water. For collagen I and collagen VI, EDTA buffer, pH 8.0, was used for antigen heat retrieval.

Immunostaining was performed using an automated stainer (Nemesis 7200, Biocare). Tissue was treated sequentially as follows: 3% hydrogen peroxide for 5 minutes, 100% SNIPER (BioCare, BS966) blocking reagent for 15 minutes, primary antibody treated for 1 hour in 10% Sniper (in TBS-T buf-

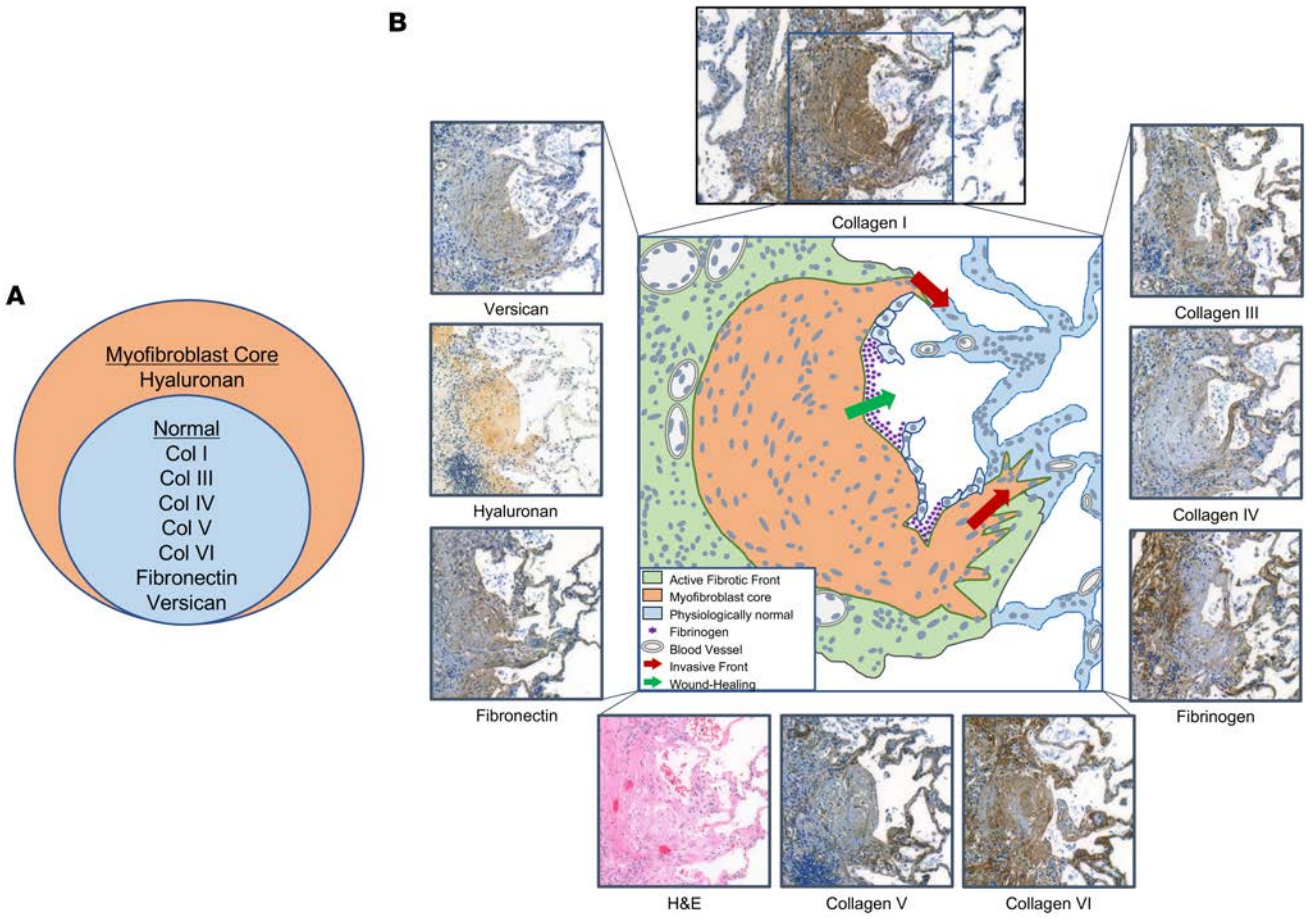


**Figure 8. A model of ECM-mediated fibrosis progression.** (**A**) The myofibroblast core of the fibroblastic focus contains collagens I, III, IV, V, and VI; fibronectin; and versican, ECM components also found in the normal lung. In addition, unlike in the normal lung, hyaluronan is ubiquitously present. (**B**) A fibroblastic focus immunostained with collagen I (top) was traced (center), with nuclei shown as circles/ovals. Surrounding the tracing, immunostaining for each component is shown for the same fibroblastic focus. The fibroblastic focus is comprised of a myofibroblast core and an active fibrotic front, defined as a highly cellular and mitotically active region at the myofibroblast core perimeter that extends into thickened alveolar septa adjacent to morphologically normal regions. This morphology is consistent with a mechanism of fibrosis progression in which myofibroblasts, at thickened alveolar septa, invade into normal regions in response to hyaluronan (red arrows). Fibrinogen marks regions of damaged/stressed epithelium where myofibroblasts begin to encroach into the airspaces, mimicking the situation in wound healing (green arrow).

fer) (see Supplemental Table 1 for list of antibodies), Novolink Polymer Detection Systems (Leica RE7270-RE, per the manufacturer's recommendations), developed for 5 minutes with DAB chromagen (Covance, SIG-31042), counterstained with hematoxylin and cover-slipped with Permount (Thermo Fisher Scientific, SP15).

For procollagen I detection, after deparaffinization, tissue was subjected to Proteinase K treatment (MilliporeSigma, 21627; working strength) for 5 minutes instead of antigen heat retrieval. Tissue was blocked in 100% Background Sniper for 1 hour, and primary antibody was reacted overnight at 4°C in 10% Background Sniper (in TBS-T). Biotinylated anti-rat antibody (Vector Laboratories, BA-4001) was used at 1:500 in 10% Background Sniper for 30 minutes, followed by Streptavidin-HRP (Covance, SIG-32254; working strength) treatment for 30 minutes and development using DAB chromagen.

*Hyaluronan detection*. Deparaffinized sections were treated with 3% hydrogen peroxide for 10 minutes, 100% Background Sniper for 1 hour, 1 μg/ml biotinylated hyaluronan-binding protein (b-HABP) (EMD; 385911) overnight at 4°C, and Streptavidin-HRP (Covance, SIG-32254) for 1 hour. Tissue was developed with DAB chromagen for 5 minutes, counterstained with hematoxylin, and cover slipped. As a test of signal specificity, deparaffinized tissue was treated with 16 U/ ml Hyaluronidase (Calbiochem, 389561) for 30 minutes in a 37°C humidified oven prior to b-HABP treatment (45).

*Histological imaging*. Stained TMA slides were subjected to an automated slide scanner (Pannoramic

250 Flash III, 3DHistech) at the University of Manchester Bioimaging Facility. Files were uploaded and cropped using Caseviewer 2.1 software (3DHistech).

*3D reconstruction*. The University of Minnesota Informatics Institute anatomically aligned and processed the images to produce the 3D reconstructions. The images were color separated using the Color Deconvolution plug-in for ImageJ (NIH) (46) to create three images: the "H" component, the "DAB" component, and a residual. The pseudocolored images were generated by combining the unmixed "DAB" components from different serial sections, each with a separate color and averaged across *Z*-slices. The single-stain color 3D volume renderings were performed using Amira (Thermo Fisher Scientific).

*Online data repository*. Data used for this manuscript are available online (47).

*Statistics*. A $\chi^2$ test was performed for all analysis. Each graph was created and calculated using Prism Graphpad software. $P < 0.05$ was considered significant.

*Study approval*. Use of patient-derived materials was approved by the University of Minnesota Institutional Review Board for Human Subjects Research (IRB 1504M68341).

## Author contributions

JH and CF designed and conducted all histological stains. AM validated histological stains and morphologies consistent with IPF. JH imaged and analyzed the histological stains. TP conducted the 3D reconstructions. JH, JS, MAS, CAH, and PBB wrote the manuscript with input from the authors. PBB, CAH, and JH conceived the project. PBB supervised the experiments.

## Acknowledgments

The authors would like to thank Lori Holm for her assistance in serially sectioning the TMA IPF blocks used for the histological stains throughout this project. This work was supported by the NIH grants R01 HL125236 (to PBB) and P01 HL091775 and R01 HL125227 (to CAH)and by funds provided by the O'Brien and Witowski families. JH was supported by core funding from the Wellcome Trust (203128/Z/16/Z).

Address correspondence to: Jeremy Herrera, University of Manchester, Oxford Road, Michael Smith Building C3225, Manchester M13 9PT, United Kingdom. Phone: 44.161.275.5078; Email: Jeremy.Herrera@manchester.ac.uk.

1. Herrera J, Henke CA, Bitterman PB. Extracellular matrix as a driver of progressive fibrosis. *J Clin Invest*. 2018;128(1):45–53.
2. Booth AJ, et al. Acellular normal and fibrotic human lung matrices as a culture system for in vitro investigation. *Am J Respir Crit Care Med*. 2012;186(9):866–876.
3. Sava P, et al. Human pericytes adopt myofibroblast properties in the microenvironment of the IPF lung. *JCI Insight*. 2017;2(24):e96352.
4. Parker MW, et al. Fibrotic extracellular matrix activates a profibrotic positive feedback loop. *J Clin Invest*. 2014;124(4):1622–1635.
5. Herrera J, et al. Dicer1 deficiency in the idiopathic pulmonary fibrosis fibroblastic focus promotes fibrosis by suppressing microRNA biogenesis. *Am J Respir Crit Care Med*. 2018;198(4):486–496.
6. Schiller HB, et al. Deep proteome profiling reveals common prevalence of MZB1-positive plasma B cells in human lung and skin fibrosis. *Am J Respir Crit Care Med*. 2017;196(10):1298–1310.
7. Korfei M, et al. Comparative proteome analysis of lung tissue from patients with idiopathic pulmonary fibrosis (IPF), non-specific interstitial pneumonia (NSIP) and organ donors. *J Proteomics*. 2013;85:109–128.
8. Korfei M, et al. Comparative proteomic analysis of lung tissue from patients with idiopathic pulmonary fibrosis (IPF) and lung transplant donor lungs. *J Proteome Res*. 2011;10(5):2185–2205.
9. White ES, Hill R, Dyal R, Wang M, Hansen K. Quantitative proteomics identifies regional differences in lung extracellular matrix. *Am J Respir Crit Care Med*. 2015;191(1):A6461.
10. Kuhn C, McDonald JA. The roles of the myofibroblast in idiopathic pulmonary fibrosis. Ultrastructural and immunohistochemical features of sites of active extracellular matrix synthesis. *Am J Pathol*. 1991;138(5):1257–1265.
11. Xia H, et al. Calcium-binding protein S100A4 confers mesenchymal progenitor cell fibrogenicity in idiopathic pulmonary fibrosis. *J Clin Invest*. 2017;127(7):2586–2597.
12. Lomas NJ, Watts KL, Akram KM, Forsyth NR, Spiteri MA. Idiopathic pulmonary fibrosis: immunohistochemical analysis provides fresh insights into lung tissue remodelling with implications for novel prognostic markers. *Int J Clin Exp Pathol*. 2012;5(1):58–71.
13. Hagood JS, et al. Loss of fibroblast Thy-1 expression correlates with lung fibrogenesis. *Am J Pathol*. 2005;167(2):365–379.
14. Raghu G, Striker LJ, Hudson LD, Striker GE. Extracellular matrix in normal and fibrotic human lungs. *Am Rev Respir Dis*. 1985;131(2):281–289.
15. Vittal R, et al. Type V collagen induced tolerance suppresses collagen deposition, TGF-β and associated transcripts in pulmonary fibrosis. *PLoS ONE*. 2013;8(10):e76451.
16. Parra ER, Teodoro WR, Velosa AP, de Oliveira CC, Yoshinari NH, Capelozzi VL. Interstitial and vascular type V collagen mor-

phologic disorganization in usual interstitial pneumonia. *J Histochem Cytochem*. 2006;54(12):1315–1325.
17. Bensadoun ES, Burke AK, Hogg JC, Roberts CR. Proteoglycan deposition in pulmonary fibrosis. *Am J Respir Crit Care Med*. 1996;154(6 Pt 1):1819–1828.
18. Garantziotis S, et al. Serum inter-alpha-trypsin inhibitor and matrix hyaluronan promote angiogenesis in fibrotic lung injury. *Am J Respir Crit Care Med*. 2008;178(9):939–947.
19. Kuhn C, Boldt J, King TE, Crouch E, Vartio T, McDonald JA. An immunohistochemical study of architectural remodeling and connective tissue synthesis in pulmonary fibrosis. *Am Rev Respir Dis*. 1989;140(6):1693–1703.
20. Broekelmann TJ, Limper AH, Colby TV, McDonald JA. Transforming growth factor beta 1 is present at sites of extracellular matrix gene expression in human pulmonary fibrosis. *Proc Natl Acad Sci USA*. 1991;88(15):6642–6646.
21. Specks U, Nerlich A, Colby TV, Wiest I, Timpl R. Increased expression of type VI collagen in lung fibrosis. *Am J Respir Crit Care Med*. 1995;151(6):1956–1964.
22. Fukuda Y, Basset F, Ferrans VJ, Yamanaka N. Significance of early intra-alveolar fibrotic lesions and integrin expression in lung biopsy specimens from patients with idiopathic pulmonary fibrosis. *Hum Pathol*. 1995;26(1):53–61.
23. Hayashi T, et al. Immunohistochemical study of metalloproteinases and their tissue inhibitors in the lungs of patients with diffuse alveolar damage and idiopathic pulmonary fibrosis. *Am J Pathol*. 1996;149(4):1241–1256.
24. Imokawa S, Sato A, Hayakawa H, Kotani M, Urano T, Takada A. Tissue factor expression and fibrin deposition in the lungs of patients with idiopathic pulmonary fibrosis and systemic sclerosis. *Am J Respir Crit Care Med*. 1997;156(2 Pt 1):631–636.
25. El-Zammar O, Rosenbaum P, Katzenstein AL. Proliferative activity in fibrosing lung diseases: a comparative study of Ki-67 immunoreactivity in diffuse alveolar damage, bronchiolitis obliterans-organizing pneumonia, and usual interstitial pneumonia. *Hum Pathol*. 2009;40(8):1182–1188.
26. Ebina M, et al. Heterogeneous increase in CD34-positive alveolar capillaries in idiopathic pulmonary fibrosis. *Am J Respir Crit Care Med*. 2004;169(11):1203–1208.
27. Yang L, et al. IL-8 mediates idiopathic pulmonary fibrosis mesenchymal progenitor cell fibrogenicity. *Am J Physiol Lung Cell Mol Physiol*. 2018;314(1):L127–L136.
28. Zhu H, et al. The role of the hyaluronan receptor CD44 in mesenchymal stem cell migration in the extracellular matrix. *Stem Cells*. 2006;24(4):928–935.
29. Shigeeda W, et al. Hyaluronic acid enhances cell migration and invasion via the YAP1/TAZ-RHAMM axis in malignant pleural mesothelioma. *Oncotarget*. 2017;8(55):93729–93740.
30. Nishiyama T, et al. Dissociation of actin microfilament organization from acquisition and maintenance of elongated shape of human dermal fibroblasts in three-dimensional collagen gel. *Matrix*. 1993;13(6):447–455.
31. Wang F, et al. In vivo stimulation of de novo collagen production caused by cross-linked hyaluronic acid dermal filler injections in photodamaged human skin. *Arch Dermatol*. 2007;143(2):155–163.
32. Turlier V, et al. Association between collagen production and mechanical stretching in dermal extracellular matrix: in vivo effect of cross-linked hyaluronic acid filler. A randomised, placebo-controlled study. *J Dermatol Sci*. 2013;69(3):187–194.
33. Xu JF, et al. Altered microRNA expression profile in synovial fluid from patients with knee osteoarthritis with treatment of hyaluronic acid. *Mol Diagn Ther*. 2015;19(5):299–308.
34. Saikia P, et al. Hyaluronic acid 35 normalizes TLR4 signaling in Kupffer cells from ethanol-fed rats via regulation of microRNA291b and its target Tollip. *Sci Rep*. 2017;7(1):15671.
35. Chambers R. Abnormal wound healing responses in pulmonary fibrosis: focus on coagulation signalling. *European Respir Rev*. 2008;17(109):130–137.
36. Ryu JK, Davalos D, Akassoglou K. Fibrinogen signal transduction in the nervous system. *J Thromb Haemost*. 2009;7 Suppl 1:151–154.
37. Jin H, Varner J. Integrins: roles in cancer development and as treatment targets. *Br J Cancer*. 2004;90(3):561–565.
38. Römpp A, Spengler B. Mass spectrometry imaging with high resolution in mass and space. *Histochem Cell Biol*. 2013;139(6):759–783.
39. Kumar S, West DC, Ponting JM, Gattamaneni HR. Sera of children with renal tumours contain low-molecular-mass hyaluronic acid. *Int J Cancer*. 1989;44(3):445–448.
40. Turley EA, Wood DK, McCarthy JB. Carcinoma cell hyaluronan as a "portable" cancerized prometastatic microenvironment. *Cancer Res*. 2016;76(9):2507–2512.
41. Day AJ, Milner CM. TSG-6: A multifunctional protein with anti-inflammatory and tissue-protective properties. Matrix Biol [published online ahead of print January 31, 2018]. https://doi.org/10.1016/j.matbio.2018.01.011.
42. Petrie RJ, Doyle AD, Yamada KM. Random versus directionally persistent cell migration. *Nat Rev Mol Cell Biol*. 2009;10(8):538–549.
43. Lynch DA, et al. Diagnostic criteria for idiopathic pulmonary fibrosis: a Fleischner Society White Paper. *Lancet Respir Med*. 2018;6(2):138–153.
44. Raghu G, et al. Diagnosis of Idiopathic Pulmonary Fibrosis. An Official ATS/ERS/JRS/ALAT Clinical Practice Guideline. *Am J Respir Crit Care Med*. 2018;198(5):e44–e68.
45. Rizzardi AE, et al. Elevated hyaluronan and hyaluronan-mediated motility receptor are associated with biochemical failure in patients with intermediate-grade prostate tumors. *Cancer*. 2014;120(12):1800–1809.
46. Schindelin J, et al. Fiji: an open-source platform for biological-image analysis. *Nat Methods*. 2012;9(7):676–682.
47. Herrera J. Supplemental Online Repository - Idiopathic Pulmonary Fibrosis: Registration of extracellular matrix components comprising the fibroblastic focus. Mendeley Data, v1. http://dx.doi.org/10.17632/6mdmym9bkz.1. Published November 6, 2018. Accessed on December 10, 2018.